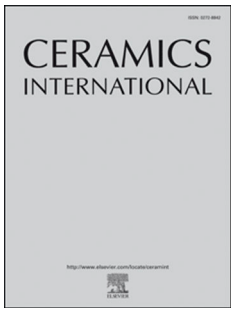

Local residual stress evolution of highly irregular thermally grown oxide layer in thermal barrier coatings

Peng Jiang, Liuyu Yang, Yongle Sun, Dingjun Li, TiejunWang

PII: S0272-8842(20)33835-9

DOI: https://doi.org/10.1016/j.ceramint.2020.12.220

Reference: CERI 27422

To appear in: *Ceramics International*

Received Date: 20 August 2020

Revised Date: 19 December 2020

Accepted Date: 22 December 2020

Please cite this article as: P. Jiang, L. Yang, Y. Sun, D. Li, TiejunWang, Local residual stress evolution of highly irregular thermally grown oxide layer in thermal barrier coatings, *Ceramics International*, https://doi.org/10.1016/j.ceramint.2020.12.220.

Ceramics International, Volume 47, Issue 8, April 2021, pp. 10990-10995
DOI:10.1016/j.ceramint.2020.12.220

Local residual stress evolution of highly irregular thermally grown oxide layer in thermal barrier coatings

Peng Jiang[1], Liuyu Yang[1], Yongle Sun[2], Dingjun Li[1,3], TiejunWang[1,*]

[1]*State Key Laboratory for Strength and Vibration of Mechanical Structures, Department of Engineering Mechanics, Xi'an Jiaotong University, Xi'an, China*

[2]*Welding Engineering and Laser Processing Centre, School of Aerospace, Transport and Manufacturing, Cranfield University, Cranfield, MK43 0AL, United Kingdom*

[3]*State Key Laboratory of Long-Life High Temperature Materials, Dongfang Steam Turbine Co., Ltd., Deyang, China.*

**Corresponding author: jiangpeng219@mail.xjtu.edu.cn*

Abstract

Local residual stress in thermally grown oxide (TGO) layers is the primary cause of failure of thermal barrier coating (TBC) systems, especially TBCs prepared by air plasma spray (APS) with a highly irregular TGO. Herein, the distribution of residual stress and the evolution of the irregular TGO layer in APS TBCs were investigated as a function of oxidation time. The stress was measured from cross-sectional micrographs and converted to the actual stress inside the coatings before sectioning. The TGO exhibited significant inhomogeneity at different locations. Stress conversion occurred across the TGO thickness; the layer near the yttria-stabilised zirconia (YSZ) component exhibited compressive stress, whereas that along the bond coat was under tensile stress. The evolution of the compressive stress is also discussed. These analyses may provide a

better understanding of the mechanism of APS TBCs.

Keywords: Thermal barrier coating, thermally grown oxide, irregular morphology, local residual stress, near *in situ* evolution

1. INTRODUCTION

The deposition of thermal barrier coatings (TBCs) is one of the most important techniques for providing insulation in gas turbines [1-3]. A typical TBC system has a multilayer structure [2]. An yttria-stabilised zirconia (YSZ) topcoat is used for thermal insulation, an MCrAlY (M = Ni, Co, etc.) bond coat acts as an oxidation-resistant layer sprayed between the topcoat and superalloy substrate, and a thermally grown oxide (TGO, predominantly α-Al_2O_3) layer is formed between the top and bond coats due to oxidation. Each layer presents fairly different thermal and mechanical parameters, leading to a complicated failure mechanism [4-10]. The main failure mode of TBCs during operation is premature delamination and spallation, and it is generally believed that the accumulated stress in TBCs is the most important factor that controls their durability. The stress originates from two components [2, 11-13]: (1) thermal expansion mismatch stress in the YSZ topcoat (with a value of several hundred megapascal), generated by the drastic temperature drop during thermal cycling, and (2) misfit and growth stresses in the TGO, which exhibits an extremely large residual compression of approximately 3–6 GPa. Although the TGO is very thin (1–10 μm), its energy density is significantly higher than that of the YSZ topcoat, which is the primary cause of failure

of TBCs.

Generally, TBCs used for gas turbine blades are fabricated by the air plasma spray (APS) method, rather than the electron beam physical vapor deposition (EB-PVD) technique used for aero-engine blades [2, 11, 14]. Consequently, the TGO of TBCs prepared by the two approaches are significantly different: the TGO of TBCs prepared by EB-PVD is relatively flat, smooth, and dense, whereas that of APS TBCs is fairly rough, tortuous, and irregular, as shown in Fig. 1. Therefore, the TGO stress field in APS TBCs is significantly less uniform and more complex [12, 15-17]. Local stress may arise near the curved portions (convex- or concave-shaped) of the TGO, resulting in the initiation and propagation of interface microcracks, eventually leading to spallation of the coating.

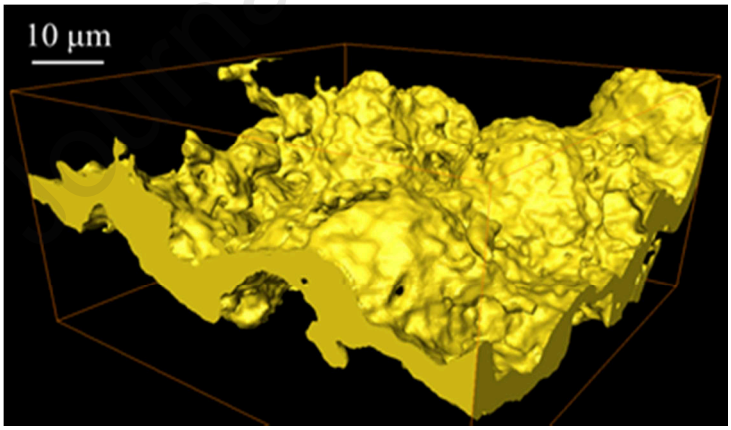

Fig. 1. Three-dimensional TGO morphology of APS TBCs, obtained by X-ray computed tomography.

Problems with the local residual stress caused by the TGO of TBCs have been extensively investigated in previous studies. Sun et al. [16, 17] proposed a spherical

model to analyse the local stress and its evolution around the cap-like portions of the TGO in APS TBCs. Bialas [18] conducted numerical simulations to study the development of interfacial cracks based on a non-uniform TGO growth and confirmed that the TGO growth results in a tensional zone within the oxide layer. Ranjbar et al. [19] built a thermo-mechanical model to evaluate the stresses induced by thermal cycling in APS TBCs as well as the effects of the TGO morphology on local interface stresses and interface microcrack nucleation. Gupta et al. [20] established a two-dimensional diffusion-based TGO growth model using the real TGO morphology extracted from cross-section micrographs and obtained stress profiles before and after TGO layer growth. Chen et al. [12] proposed a complex numerical model using temperature-dependent material parameters to study the influence of inhomogeneous TGO thickness on the residual stress distribution in APS TBCs. Tomimatsu et al. [21] measured the stress distributions in the regular TGO layer of EB-PVD TBCs and found that the stress distribution is not uniform, that is, the stress near the ceramic topcoat is lower than that close to the metal bond coat. Wang et al. [22, 23] experimentally investigated the residual stress and its TGO field in EB-PVD TBCs and monitored local stress changes during thermal cycling.

However, most studies have focused on the effect of the TGO on the surrounding coatings, and few studies have investigated the relationship between the highly irregular TGO morphology and its intrinsic local stress in APS TBCs. In particular, no experimental evidence has been reported on the synchronous *in situ* evolution of the

TGO and local residual stress. The primary goal of this work is to track the evolution of the local residual stress and morphology of highly irregular TGO in APS TBCs. We performed *in situ* measurement of the residual stress distribution and evolution of a highly irregular TGO in a polished region with a cross-section of 300 × 60 μm^2. The TGO residual stress within the coatings was then corrected based on the results of the cross-section analysis. The TGO morphology and interface microstructures, including cracks and delamination, were simultaneously monitored. Finally, we analysed the effects of the local stress field.

2. EXPERIMENTAL

The substrate used in this work was a nickel-based superalloy IN718. A 120-μm bond coat was fabricated by high-velocity oxygen fuel flame spraying, using commercial NiCoCrAlY powders (45–75 μm, Ni: 32 wt%, Co: 38.5 wt%, Cr: 21 wt%, Al: 8 wt%, Y: 0.5 wt%, Sulze-Metco). A 500 μm topcoat was fabricated via the APS method using commercial YSZ powders (45–100 μm, purity 99.99%, Institute of Process Engineering, Chinese Academy of Science). Before spraying the bond coat, the substrates were grit-blasted using aluminium oxide particles using a high-pressure suction blasting system (model STR-1212, STELLE, China). The average surface roughness of the blasted substrate was controlled at approximately 4.5–5.5 μm using a surface roughness tester (model SJ-310, Mitutoyo, Japan). The bond coat surface was not grit blasted before spraying the topcoat, and the roughness was measured as 4–5 μm.

The specimen was then cut into small blocks with dimensions of 4 mm × 4 mm × 3.62 mm using a wire-cutting device (model STX-202A, KEJING, China). The detailed parameters used for thermal spraying can be found in previous studies [24, 25].

Four small TBC blocks were chosen for the tests. Three were oxidized at 1150 °C in a laboratory muffle furnace (KSL-1700X, KEJING, China) from the as-sprayed state to spallation. The total oxidation time was determined to be 120 h; delamination occurred, and the residual stress substantially decreased. The remaining small block was used for the residual stress measurement. At different oxidation times (20, 40, 80, and 120 h), the specimens were temporarily removed from the furnace and mounted in cold resin at room temperature. The cross-section was then polished with abrasive paper. It should be noted that we did not detect the stress and morphology before oxidation, because the TGO layer was very thin (usually no more than 0.5 μm) after thermal spraying, and the spectrum signal was too weak to be detected. To prevent TGO growth normal to the cross-section and ensure the in-situ tracking of the same location at each time, minimal polishing was conducted within 1 min; thus, stress induced by polishing could be ignored. Next, the residual TGO stress was measured from a cross-section with an area of approximately 300 μm × 60 μm, as shown in Fig. 2. The selected measured region was located in the middle of the sample, which was helpful to avoid the edge effect. This was a representative region in APS TBCs, containing many typical TGO morphologies, such as convex interfaces and concave interfaces. The morphology and interface micro-cracks were inspected using a scanning electron microscope (SU3500,

Hitachi, Japan) equipped with an energy dispersive X-ray (EDX) spectrometer. At the end of each measurement, the specimens were returned to the furnace for the next oxidation cycle.

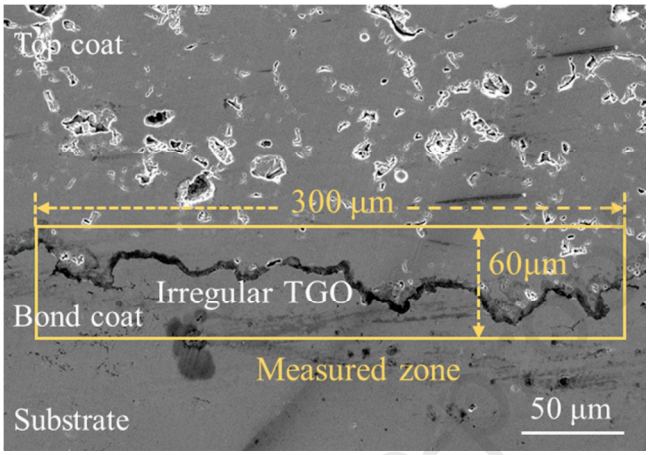

Fig. 2. Cross-sectional zone selected for residual stress measurements in APS TBCs (area: 300 μm × 60 μm)

The photoluminescence piezo-spectroscopy (PLPS) method was used to map the TGO residual stress and monitor its evolution. This is currently regarded as the most successful and accurate non-destructive method, whereas the residual stress was obtained from the stress-induced frequency shift of Cr^{3+} impurities in TGO. A Raman spectrometer (LabRAM HR Evolution, HORIBA, France) with a 532-nm laser operating at 75 mW was used to excite the Cr^{3+} ions and obtain the luminescence spectrum. The spectral resolution was set at 0.3 cm^{-1} with a grating of 1800 g/cm. The laser beam was focused on the sample using a 50× objective lens, and the spot size of the laser was approximately 1 μm. The spatial resolution was also set to 1 μm for a more accurate TGO mapping. The total measured zone data included approximately

18,000 points. The acquisition time of each point was 0.5 s at a 0.1% laser power, and the total measurement time was approximately 2.5 h. For the analysis, a Lorentz curve was used to fit the spectrum and determine the peak position. The spectral peak of Cr^{3+} ions shifts to shorter wavelengths under compressive stress. The peak shift could be determined by comparing it to the reference peak position in the stress-free TGO, whose average value was 14,435.7 cm^{-1}.

The following relationship between peak shift and stress was used to convert the shift values to average local residual stress mappings [26]:

$$\sigma_{TGO} = (\nu_s - \nu_0)/\Pi_{ii} = \frac{1}{3} \times (\sigma_{xx} + \sigma_{yy} + \sigma_{zz}) \quad (1)$$

where ν_s and ν_0 are the peak positions of the Cr^{3+} luminescence spectrum of the TGO under residual stress and in the stress-free state, respectively; σ_{ij} is the stress state on the crystallographic basis of the host crystal, Π_{ii} is the trace of the piezo-spectroscopic coefficient tensor. A value of 7.59 cm^{-1}/GPa was used for the R1 peak [27], and z direction represents the through-thickness direction.

In the present measurements, peak shifts were detected from the polished transverse section of the TGO layer. Thus, free-edge (x-z section) effects should be considered for the conversion between the peak shift and TGO layer stress.

Owing to the lack of individual values of stress components (only the average local residual stress was obtained by PLPS), σ_{xx}, σ_{yy}, and σ_{zz}, it is difficult to realise stress conversion. Provided that the TGO thickness (in the z direction) is very small, the TGO can be assumed to be flat [28]. Thus, under plane stress conditions, the stress

component σ_{zz} can be assumed to be zero ($\sigma_{zz} \approx 0$), and the stress components σ_{xx} and σ_{yy} are equal, that is, $\sigma_{xx} = \sigma_{yy}$. The TGO stress inside the TBC system is then expressed as

$$\sigma_{TGO\cdot inner} = \frac{2}{3}\sigma_{yy}, \quad (2)$$

The measured stress from the x–z section can be written as [28]

$$\sigma_{TGO\cdot section} = \frac{1}{3} \times (\sigma_{xx} + \Omega\sigma_{yy} + \sigma_{zz}), \quad (3)$$

where Ω is the correlation factor which cancels the free-edge effects on the measured average stress of the TGO layer; it was experimentally determined as 0.25 in a previous study [28]. Under the plane stress condition, Eq. (3) can thus be written as [28]

$$\sigma_{TGO\cdot section} = \frac{1+\Omega}{3}\sigma_{yy}. \quad (4)$$

Finally, the TGO stress within the coatings can be written as

$$\sigma_{TGO\cdot inner} \approx \frac{2}{1+\Omega}\sigma_{TGO\cdot section}. \quad (5)$$

3. RESULTS AND DISCUSSION

Figure 3 shows the colour-rendered cross-sectional microstructure and EDX images at the same location of APS TBCs after oxidation for 20, 40, 80, and 120 h. The NiCoCrAlY bond coat and the YSZ topcoat are coloured light blue and green, respectively. The irregular TGO at the topcoat/bond-coat interface is marked in dark red. The *in situ* evolution of the TGO growth and interface cracks is evident. Up to 80 h (Fig. 3a–c), the TGO grew rapidly while the interface remained intact, and no interface micro-cracks were observed. Subsequently, as shown in Fig. 3d, the TGO growth rate

slows down. A major interface crack occurs at the bottom of the topcoat above the TGO, leading to the final coating spallation.

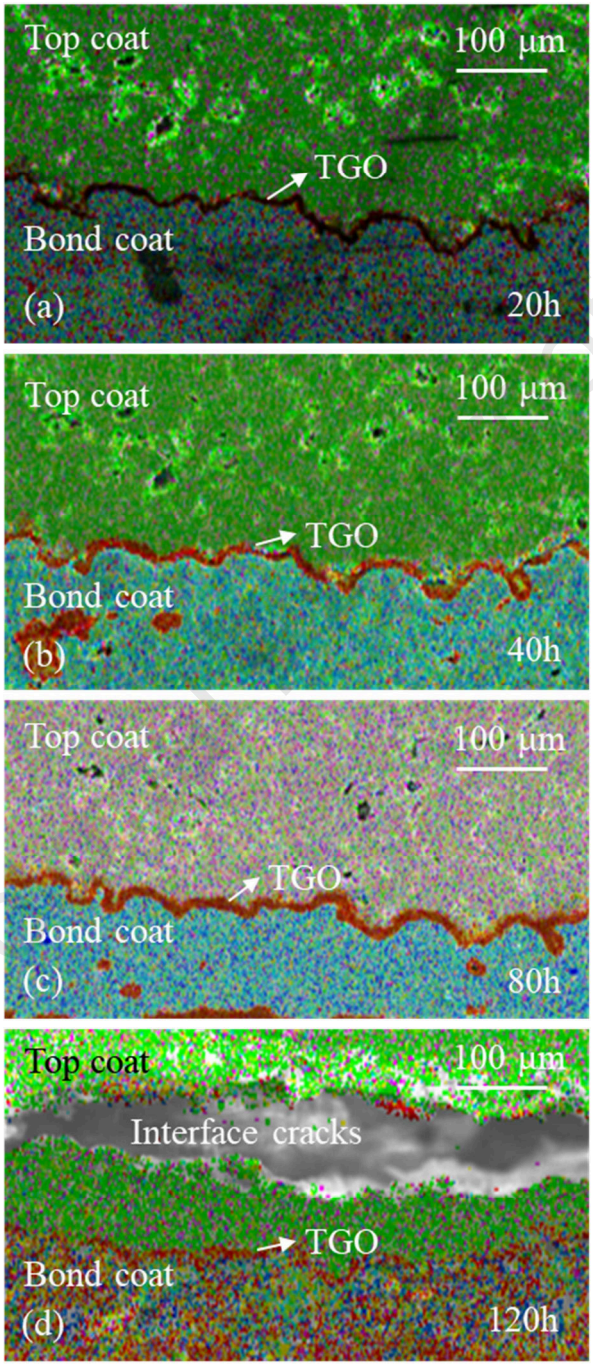

Fig. 3. Cross-sectional EDX maps of TBCs at different oxidation times, showing *in situ* TGO growth and occurrence of interface cracks.

Figure 4 shows the residual TGO stress distribution on the polished cross-section of the selected TBC specimen and its evolution at the same location. The mappings correspond to the cross-sectional results at different oxidation times, as shown in Fig. 3. The relative proportions of TGO residual stress at different oxidation times are shown in Fig. 5. The stress value (positive in tension) was estimated by Eq. 2, showing the actual stress levels inside an uncut TBC specimen. After the first 20 h of oxidation, as shown in Figs. 4a and 5a, the TGO exhibits both compressive and tensile stresses at different locations. Approximately 67% of locations are under 0–1 GPa compression, 5% are under 1–2 GPa compression, and the others are under tension. The stress appears to change across the TGO thickness, with the layer near the YSZ exhibiting compressive stress (0–1 GPa), while some concave-interface regions near the bond coat show tensile stress (0–3 GPa). Furthermore, tensile stress is likely to accumulate at TGO positions with downward concavity. This is very different from the results reported for EB-PVD TBCs, where the TGO stress distribution was nearly uniform [22] and only a few positions near the TGO/YSZ interface were under tensile stress [21]. This may be due to the highly irregular TGO morphology and local imperfections in the surrounding coatings. The present results provide sufficient evidence to show that the stress in the irregular TGO of APS TBCs is non-uniform and that compressive and tensile stresses coexist. After 40 h of oxidation (Figs 4b and 5b), the TGO becomes thicker, and is accompanied by stress accumulation. The proportion of 0–1 GPa compression zones decreases, while that of 1–3 GPa compression zones increases; the percentage of tensile

stress remains unchanged. The TGO stress level in the original compressive-stress zones near the YSZ increases to 1–3 GPa. Concurrently, some newly formed compressive-stress zones are observed in the original tensile-stress zones near the bond coat, although they are very small, possibly due to the following factors: on the one hand, the constraint of the surrounding YSZ topcoat and NiCoCrAlY bond coat increases significantly as the TGO increases, resulting in an overall upward compressive stress in the entire TGO layer; on the other hand, the composition of the TGO may change during growth. Shillington and Clarke [29] reported that the formation of Cr_2O_3 in the TGO layer may lead to a change in the TGO stress. It should be noted that a new tensile-stress area is generated in the original compressive-stress area. This may also be due to variation in the TGO compositions. After 80 h of oxidation (Figs 4c and 5c), the proportion of tensile stress zones drastically reduces to approximately 10%, and most of the TGO profile exhibits large compressive stresses with estimated values of 1–4 GPa. The remaining tensile stress remains localised at the downward concavity positions of the TGO. After 120 h of oxidation (Figs 4d and 5d), interface cracks form and delamination occurs (Fig. 3d). The residual TGO stress thus significantly reduces, and ~55% of compression zones under 0–1 GPa and ~10% of tensile stress zones under 0–1 GPa remain until coating spallation. Moreover, due to the disappearance of the coating constraints, the state of the stress-converted zones in the first 80 h changes again from compression to tensile stress.

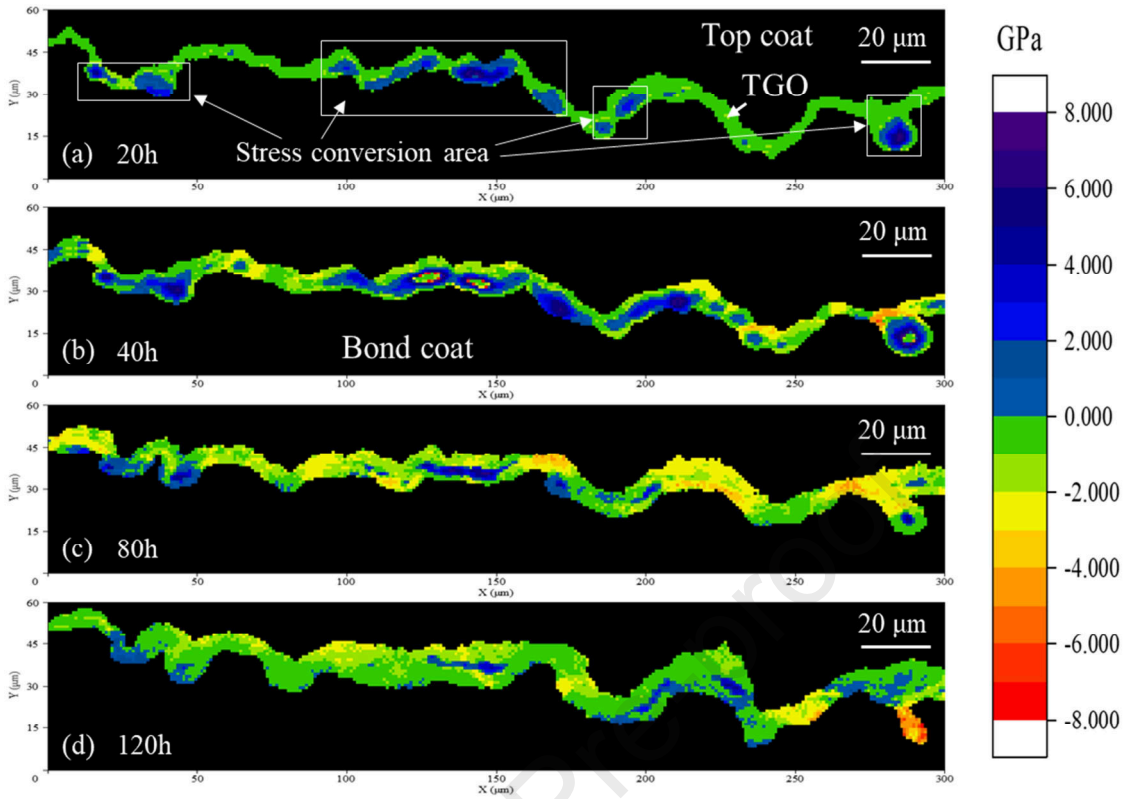

Fig. 4. Residual stress distribution (positive in tension) and evolution of TGO in a polished cross-section at a specific location of a selected APS TBCs specimen.

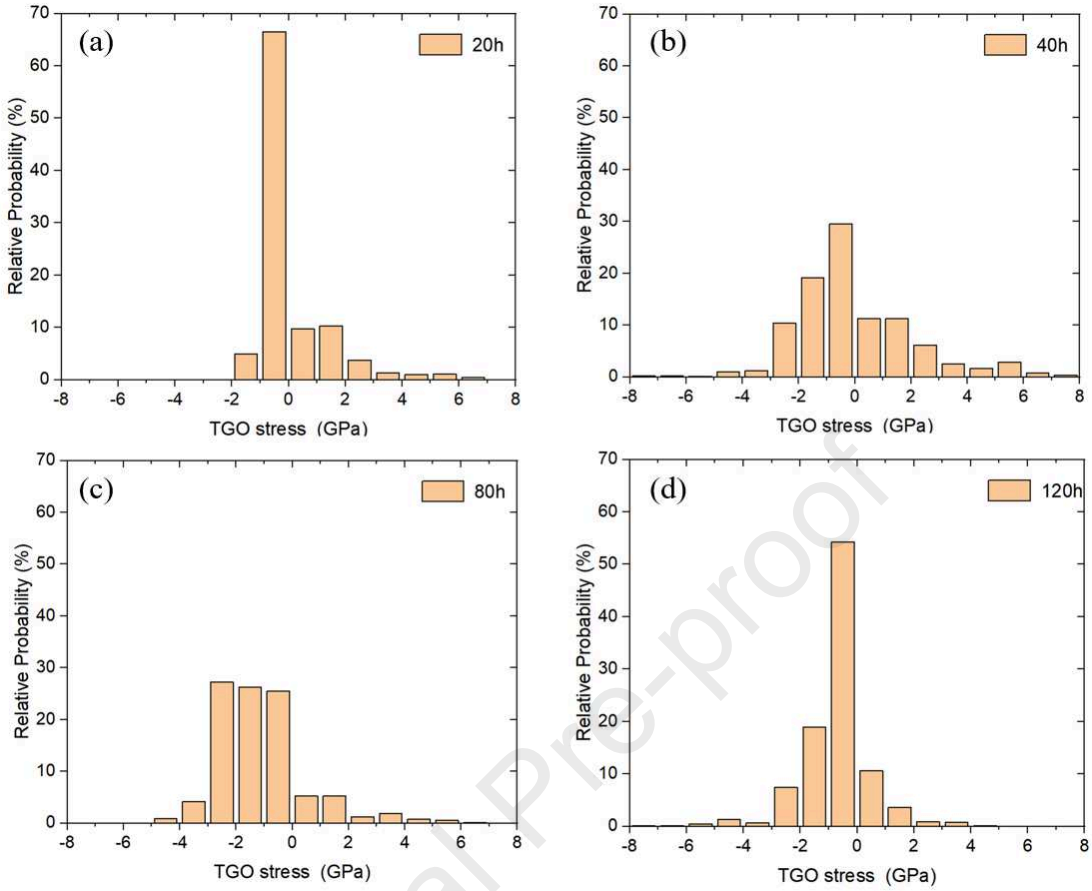

Fig. 5. Relative probability of TGO residual stress (positive in tension) at different oxidation times.

Figure 6 shows the synchronous variation in the TGO thickness and average residual stress as a function of oxidation time. The figure reveals that the TGO thickness rapidly increases to approximately 7 μm during the first 80 h before slowing down. Concurrently, the standard deviation shows a significant increase during the entire oxidation period, indicating a continuous increase in the irregularity and heterogeneity of the TGO. The average residual stress changes from 0.26 GPa (tension) at 20 h to 0.06 GPa (compression) at 40 h and then to 1.1 GPa (compression) at 80 h. Next, the stress rapidly drops to approximately 0.66 GPa in compression, and interface cracks are

formed. Notably, the average cross-sectional stress is lower than that measured from the top surface across the YSZ topcoat. This may be due to the luminescence signals detected from the surface originating primarily from the upper region of the TGO close to the YSZ layer and represents compressive stress. The mean cross-sectional stress values are the average of the compressive and tensile stresses of the entire TGO. In addition, lower TGO stresses were measured in the zone with interface cracks. Therefore, if changes in the TGO local stress can be accurately measured from the top surface, monitoring the conditions of TBCs could be based on the analysis of the TGO stress.

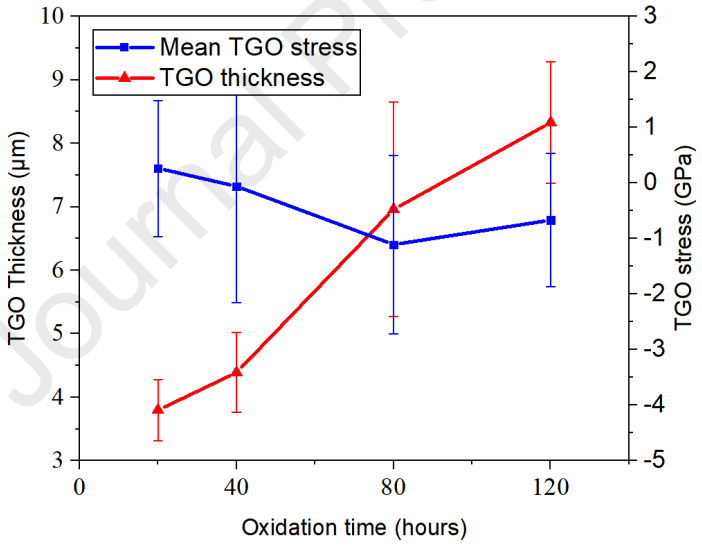

Fig. 6. Synchronous TGO thickness changes and the average residual stress (positive in tension) with increasing oxidation time.

4. Conclusion

We performed *in situ* measurements of the residual stress of a highly irregular TGO

in APS TBCs with a large, polished cross-section of 300 × 60 μm^2. The cross-sectional stress values were then converted to internal stresses of the coating before sectioning. Then, we obtained the local stress distribution in the full TGO and monitored its evolution with the oxidation time. The main conclusions can be summarised as follows:

(1) Although TGO exhibits overall compressive stress, it presents significant inhomogeneity at different locations. Stress conversion appears to occur across the TGO thickness, with the layer near the YSZ exhibiting compressive stress and some concave-interface regions near the bond coat showing tensile stress (0–3 GPa). These findings are markedly different from the results obtained for EB-PVD TBCs.

(2) With increasing oxidation time, the compressive stress in the TGO region near the YSZ topcoat increases from approximately 0 to 1 GPa at 20 h to 1–3 GPa at 40 h, and then to 1–4 GPa at 80 h. After, the stress drops rapidly owing to the occurrence of interface cracks. The tensile stress in the TGO region close to the bond coat remains at 0–3 GPa until the TBC spallation. At the same time, the proportion of tensile stress zones decreased throughout the experiment.

(3) After the failure of the TBC, tensile stress zones still existed until the spallation of the coating. Furthermore, owing to the disappearance of the coating constraints, the state of some stress-converted zones before 80 h returns from compression to tensile stress.

(4) The average stress measured on the cross sections is lower than that estimated on the top surface across the YSZ topcoat. This may be due to the luminescence signals

detected from the top surface originating primarily from the upper TGO region close to the YSZ layer and denotes compressive stress.

ACKNOWLEDGEMENT

This work was supported by the National Natural Science Foundation of China (11902240), a China Postdoctoral Science Foundation-funded project (221055), funding from the State Key Laboratory of Long-life High Temperature Materials and the Fundamental Research Funds for the Central Universities.

REFERENCES

[1] Poerschke DL, Jackson RW, Levi CG. Silicate deposit degradation of engineered coatings in gas turbines: progress toward models and materials solutions[J]. *Annual Review of Materials Research.* 2017, 47(1):annurev-matsci-010917-105000.

[2] Campo E, Lupinc V. High temperature structural materials for gas turbines[J]. *Metallurgical Science & Tecnology.* 2013.

[3] Padture NP, Gell M, and Jordan EH. Thermal barrier coatings for gas turbine engine applications, *Science.* 2002;296:280.

[4] Schlichting KW, Padture NP, Jordan EH, et al. Failure modes in plasma-sprayed thermal barrier coatings, *Mat Sci Eng A.* 2003;342:120-130.

[5] Kumar V and Balasubramanian K. Progress update on failure mechanisms of advanced thermal barrier coatings: A review, *Prog Org Coat.* 2016;90:54-82.

[6] Evans AG, Mumm DR, Hutchinson JW, et al. Mechanisms controlling the durability of thermal barrier coatings. *Prog Mater Sci.* 2001;46:505-553.

[7] Spitsberg IT, Mumm DR, Evans AG. On the failure mechanisms of thermal barrier coatings with diffusion aluminide bond coatings[J]. *Materials Science & Engineering A.* 2005, 394(1-2):176-191.

[8] Li GR, Wang LS, Zhang WW, et al. Tailoring degradation-resistant thermal barrier coatings based on the orientation of spontaneously formed pores: From retardation to self-improvement[J], *Composites Part B: Engineering.* 2020, 181:1359-8368.

[9] Liu MJ, Yang GJ, Li CJ, et al. Evaporation of droplets in plasma spray-physical vapor deposition based on energy compensation between self-cooling and plasma heat transfer[J]. *Journal of Thermal Spray Technology.* 2017, 26(7): 1641-1650.

[10] Li QL, Song P, Dong Q, et al. Effect of partial crystallization of an amorphous layer on the mechanical properties of ceramic/metal-glass coating by thermal spraying[J], *Ceramics International.* 2019, 45(15):18803-18813.

[11] Wang TJ, Fan XL, Sun YL, et al. The stresses and cracks in thermal barrier coating system: A review[J]. *Acta Mechanica Solida Sinica.* 2016, 37(6):477-517.

[12] Zhi C, Hongmei H, Kai Z, et al. Influence of inhomogeneous thermally grown oxide thickness on residual stress distribution in thermal barrier coating system[J]. *Ceramics International.* 2018:S027288421831575X.

[13] Jiang P, Fan XL, Sun YL, et al. Thermal-cycle dependent residual stress within the crack-susceptible zone in thermal barrier coating system[J]. *Journal of the*

American Ceramic Society. 2018, 101(9).

[14] Sadowski T, Przemysław, Golewski. Loadings in thermal barrier coatings of jet engine turbine blades[J]. *Springerbriefs in Applied Sciences & Technology.* 2016.

[15] Fukuchi T, Eto S, Okada M, et al. Evaluation of applicability of compact excitation light source to detection of thermally grown oxide layer in thermal barrier coating for gas turbines[J]. *Electrical Engineering in Japan.* 2015, 190(1):1-8.

[16] Sun YL, Zhang WX, Li JG, et al. Local stress around cap-like portions of anisotropically and nonuniformly grown oxide layer in thermal barrier coating system[J]. *Journal of Materials Science.* 2013, 48(17):5962-5982.

[17] Sun YL, Li JG, Zhang WX, et al. Local stress evolution in thermal barrier coating system during isothermal growth of irregular oxide layer[J]. *Surface & Coatings Technology.* 2013, 216(Complete):237-250.

[18] Bialas M. Finite element analysis of stress distribution in thermal barrier coatings[J]. *Surface & Coatings Technology.* 2008, 202(24):6002-6010.

[19] Ranjbar-Far M, Absi J, Mariaux G, et al. Simulation of the effect of material properties and interface roughness on the stress distribution in thermal barrier coatings using finite element method[J]. *Materials & Design.* 2010, 31(2):772-781.

[20] Gupta M, Eriksson R, Sand U, et al. A diffusion-based oxide layer growth model using real interface roughness in thermal barrier coatings for lifetime assessment[J]. *Surface & Coatings Technology.* 2015, 271:181-191.

[21] Tomimatsu T, Zhu S, Kagawa Y. Effect of thermal exposure on stress distribution in

TGO layer of EB-PVD TBC[J]. *Acta Materialia.* 2003, 51(8):2397-2405.

[22] Wang X, Wu RT, Atkinson A. Characterisation of residual stress and interface degradation in TBCs by photo-luminescence piezo-spectroscopy[J]. *Surface & Coatings Technology.* 2010, 204(15):2472-2482.

[23] Wang X, Atkinson A, Chirivi L. Evolution of stress and morphology in thermal barrier coatings[J]. *Surface & Coatings Technology.* 2010, 204(23):3851–3857.

[24] Jiang P, Fan XL, Sun YL, et al. Competition mechanism of interfacial cracks in thermal barrier coating system, *Materials & Design.* 2017;132:559-566.

[25] Jiang P, Fan XL, Sun YL, et al. Bending-driven failure mechanism and modelling of double-ceramic-layer thermal barrier coating system[J]. *International Journal of Solids and Structures.* 2018, 130: 11-20.

[26] Christensen RJ, Lipkin DM, Clarke DR, et al. Nondestructive evaluation of the oxidation stresses through thermal barrier coatings using Cr^{3+} piezospectroscopy[J]. *Applied Physics Letters.* 1996, 69(24):3754.

[27] Manero A, Selimov A, Fouliard Q, et al. Piezospectroscopic evaluation and damage identification for thermal barrier coatings subjected to simulated engine environments[J]. *Surface and Coatings Technology.* 2016:S0257897216309410.

[28] Kitazawa R, Kakisawa H, Kagawa Y. Anisotropic TGO morphology and stress distribution in EB-PVD Y2O3-ZrO2 thermal barrier coating after in-phase thermo-mechanical test[J]. *Surface and Coatings Technology*, 2014, 238:68-74.

[29] Shillington EAG, Clarke DR. Spalling failure of a thermal barrier coating

associated with aluminum depletion in the bond coat[J]. *Acta Materialia.* 1999, 47(4):1297-1305.

Figure captions

Figure 1. Three-dimensional TGO morphology of APS TBCs obtained via X-ray computed tomography.

Figure 2. Cross-sectional zone selected for residual stress measurement in APS TBCs (area: 300 μm × 60 μm)

Figure 3. Cross-sectional EDX map of TBCs at different oxidation times, showing *in situ* TGO growth and occurrence of interface cracks.

Figure 4. Residual stress distribution (positive in tension) and evolution of TGO on the polished cross-section at a specific location of a selected APS TBCs specimen.

Figure 5. Relative probability of TGO residual stress (positive in tension) at different oxidation times.

Figure 6. Synchronous TGO thickness changes and the average residual stress (positive in tension) with increasing oxidation time.

Declaration of Interest statement

☒ The authors declare that they have no known competing financial interests or personal relationships that could have appeared to influence the work reported in this paper.

☐The authors declare the following financial interests/personal relationships which may be considered as potential competing interests: